Self-organized Models of Selectivity in Calcium Channels

Janhavi Giri[1, 2], James E. Fonseca[1], Dezső Boda[3, 4], Douglas Henderson[4], Bob Eisenberg[1*]

[1] Department of Molecular Biophysics and Physiology, Rush University, Chicago, IL 60612

[2] Department of Bioengineering, University of Illinois at Chicago, Chicago, IL 60607

[3] Department of Physical Chemistry, University of Pannonia, P. O. Box 158, H-8201 Veszprém, Hungary

[4] Department of Chemistry and Biochemistry, Brigham Young University, Provo, UT 84602

October 18, 2010

Key words: selectivity, calcium channel, self-organized, induced fit

File Name: Flexibility-October-18-1-2010.doc

[*] Author to whom correspondence should be addressed. Email address: beisenbe@rush.edu

ABSTRACT

The role of flexibility in the selectivity of calcium channels is studied using a simple model with two parameters that accounts for the selectivity of calcium (and sodium) channels in many ionic solutions of different composition and concentration using two parameters with unchanging values. We compare the distribution of side chains (oxygens) and cations (Na^+ and Ca^{2+}) and the integrated quantities. We compare the occupancies of cations Ca^{2+}/ Na^+ and linearized conductance of Na^+. The distributions show a strong dependence on the locations of fixed side chains and the flexibility of the side chains. Holding the side chains fixed at certain predetermined locations in the selectivity filter distorts the distribution of Ca^{2+} and Na^+ in the selectivity filter. However, integrated quantities—occupancy and normalized conductance—are much less sensitive. Our results show that some flexibility of side chains is necessary to avoid obstruction of the ionic pathway by oxygen ions in 'unfortunate' fixed positions. When oxygen ions are mobile, they adjust 'automatically' and move 'out of the way', so they can accommodate the permeable cations in the selectivity filter. Structure is the computed consequence of the forces in this model. The structures are self-organized, at their free energy minimum. The relationship of ions and side chains vary with ionic solution. Monte Carlo simulations are particularly well suited to compute induced fit, self-organized structures because the simulations yield an ensemble of structures near their free energy minimum. The exact location and mobility of oxygen ions have little effect on the selectivity behavior of calcium channels. Seemingly, nature has chosen a robust mechanism to control selectivity in calcium channels: the first order determinant of selectivity is the density of charge in the selectivity filter. The density is determined by filter volume along with the charge and excluded volume of structural ions confined within it. Flexibility seems a second order determinant.

These results justify our original assumption that the important factor in Ca^{2+} vs Na^+ selectivity is the density of oxygen ions in the selectivity filter along with (charge) polarization (i.e., dielectric properties). The assumption of maximum mobility of oxygens seems to be an excellent approximate working hypothesis in the absence of exact structural information. These conclusions, of course, apply to what we study here. Flexibility and fine structural details may have important role in other properties of calcium channels that are not studied in this paper. They surely have important roles in other channels, enzymes, and proteins.

INTRODUCTION

Selectivity arises from the interactions of ions and side chains of proteins constrained by the geometry and properties of the rest of the protein, and the surrounding bathing solutions. For a long time—as long as the issue of selectivity has been considered by biologists—we have believed that selectivity depends on the detailed structure of the binding sites for ions. Selectivity has been thought to depend on the exact atomic arrangements of side chains, ions, and other nearby molecules [1, 2]. The selectivity of the calcium channel we consider here is particularly important because of the enormous importance of the channel [3-21]. The L-type calcium channel that we have in mind controls the contraction of the heart and signaling in skeletal muscle. Few channels are more important than the calcium channel because calcium concentration inside cells is used as a signal in almost every tissue of an animal.

It has come as a surprise that a model of selectivity that includes only a few features of the atomic structure has been able to describe the selectivity properties of calcium and sodium channels very well, in all solutions over a wide range of conditions, with only two adjustable parameters using crystal radii of ions [22, 23]. This model is skeletal in its simplicity, representing side chains as charged spheres unrestrained by connections to the surrounding protein. This model represents the selectivity filter of calcium and sodium channels as cylinders containing spherical structural ions (modeling the terminal groups of side chains) free to move within the cylinder but unable to leave it (Figure 1). Note that water is present in this model only as a dielectric: the primitive implicit solvent [24-48] model of ionic solutions is used and extended into the channel. The *question* is how can this simple model possibly work, given that it includes no detail of the protein structure, and uses only a crude representation (to put it kindly) of the side chains and their interaction with ions.

The *answer* we give is that the model works because it captures the features of the binding sites of calcium and sodium channels that biology actually uses to produce selectivity. Many other physical phenomena could be used to produce selectivity, and probably are in other types of channels, transporters, enzymes, and proteins, let alone physical systems in general. It seems here however that biology has used only the simplest, the competition between electrostatic forces and volume exclusion in very concentrated systems of ions and side chains.

The two cations Ca^{2+} and Na^{+} that compete for the channel arrive from a bath of a given composition and mix with side chains of the channel protein in our model. The winner of the competition is the ionic species whose binding minimizes the free energy $F = U - TS$. Electrostatic attraction between the side chains and the cations decreases the energy U, while competition for space in the crowded selectivity filter chiefly influences the $-TS$ term. The entropic term is most directly influenced by the flexibility of side chains. Indirectly, of course, everything is influenced by everything. The *U* and *–TS* terms are not uncoupled, of course [49], but separating *U* and *–TS* terms provides a useful framework to understand selectivity.

Our model assumes a large mobility (flexibility) of the terminal groups (8 half-charged oxygen ions, in this paper) of side chains. In reality, the movement of side chains is restricted because they are tethered to the polypeptide backbone of a protein. Side chains of acidic and basic residues in real proteins are not fully rigid (though they are not entirely mobile either) and have considerable mobility during thermal motion.

The goal of this paper is to study the effect of the flexibility of the side chains on physical quantities computed by Monte Carlo simulation. The basic quantities computed by the simulation are the profiles of spatial distribution of the various ionic species. These distributions, as expected, are very sensitive to restrictions in the mobility of oxygen ions.

Integration of the ionic profiles provides quantities comparable to experiments. These integral properties characterize selectivity from two profoundly different points of view.

(1) The integral of the ionic profile (of a given species) itself over a given volume (of the selectivity filter, for example) describes the *binding affinity* of the given ionic species to this volume. This quantity—that we call ‘occupancy’—is proportional to the probability that a given ionic species binds to the selectivity filter in competition with other kind of ions. Occupancy is a result of minimized free energy, an equilibrium concept, but occupancy exists in non-equilibrium systems as well, of course. It just must be computed by a different theory in that case, one that includes nonequilibrium parameters (like conductance) and spatially nonuniform boundary conditions.[50, 51]

(2) The resistance of the channel is the sum of the resistance of a series of (infinitesimally thin) discs, as described precisely later in Methods section. Resistance is a more dynamic variable than occupancy. Each disc has resistance determined by the amount and mobility of the

ions in the disc. The amount is proportional to the reciprocal of the concentration of ions, times the volume of the disc. The sum is actually the integral of the reciprocal of the profile of ionic concentration over a length of the ionic pathway. The integral is proportional to the resistance of that length to the current of the ionic species in question. This resistance describes the selectivity of ion channels directly measurable from measurements of current or flux through channels under near equilibrium conditions. It is more sensitive to local variations in the ionic profiles than occupancy. It is expected, therefore, that conductance is more sensitive to variations in flexibility of side chains too.

We will change the flexibility of the oxygen ions in different ways and analyze how the physical quantities mentioned above change as flexibility is changed. We obtain quite different behavior for the profiles, occupancies, and conductances as a function of varying flexibility.

An important result of analysis of this model is that the locations of ions and side chains have a 'self adjusting' nature as ion concentrations are changed in the bath, or the nature of the side chains is altered, for example, from EEEE to EEEA in a calcium channel or DEKA to DEEA in a sodium channel. Side chains are mobile in our model and so they change their distribution as parameters of the model change. In this picture, the structure of the binding site is a computed consequence of thermodynamic and geometrical constraints and all the forces present in the system. Thus, by *'structure*' we mean the equilibrium profiles of spatial distribution of concentration of all the ions obtained as ensemble averages of converged simulations. This structure obviously changes as experimental conditions change.

The sensitivity of the structure to the location and flexibility of side chains helps answer the general paradox "How can a model without a detailed structure account for complicated properties of two different types of channels under so many conditions?" The answer to the question is that the model computes the structure. The channel structure is different in different conditions because of the sensitivity of spatial distributions. Thus, biological properties that are sensitive to structure will be sensitive to location and flexibility of side chains. Integrated properties like conductance are not so sensitive.

In other words, the model of selectivity is an induced fit model, in which the structure of the binding site is induced by all the forces in the system, depending on the ion concentrations in the bath, and the other parameters of the problem. The fit of the side chains to the ions is induced

by the minimization of the free energies of the system. The model is a self organized model. In our model, the only energies that determine the structure are electrostatic and excluded volume. No energies with a more chemical flavor are included in the present version of the model.

Unfortunately, we do not know anything about the actual locations of side chains in real calcium and sodium channels because X-ray structures are unavailable. It is possible to hypothesize the locations assuming various homologies with the known structure of the KcsA potassium channel [52, 53]. We followed a different route as described in the Model section.

We conclude that ionic distribution profiles are sensitive functions of locations of immobilized side chains and their flexibility. Occupancy, on the other hand is less sensitive to flexibility because its first order determinant is the density of ions in the selectivity filter as we established earlier [54, 55]. Conductance, the most interesting quantity of the three, lies in between because it depends on both occupancy (the number of available charge carriers) and fine details in the distribution profiles. The conductance of a single channel of fixed diameter depends on the sum of many differential 'resistors' because it measures the 'series resistance' of the single channel. The conductance depends on the reciprocal of the concentration for this reason and is very sensitive to high resistance obstructions in the permeation pathway even if they occur over a tiny length. These high resistances are produced by the low concentrations of mobile ions in the depletion zones in the ionic profiles [56]. Depletion zones are responsible for many of the most important properties of transistors [57-59]. Transistors and channels involve quite similar physics and are described by quite similar equations, but the charge carriers of transistors are points with no size.

If three dimensional structures for calcium and sodium channels become available, the information gained must be built into our model. Until then, our approach—that allows the side chains to find their optimal distribution automatically in the simulation—seems to be a good way to proceed. It allows us to construct a functional skeletal model that fits a wide range of data from two channel types under many conditions with only two parameters. It makes understanding of permeation and selectivity mechanisms of real calcium and sodium channels possible, if permeation and selectivity are viewed as outputs of that simplified model.

METHODS

Model of Channel and Electrolyte

We use a reduced model to represent the L-type calcium channel because a crystallographic structure is not available. We know from the experimental literature that Ca^{2+} selectivity in this channel is determined and regulated by the four glutamates of the pore lining loops which form the selectivity filter [60-63]. The negatively charged carboxyl (COO^-) side chains of these glutamates extend into the selectivity filter region of the channel [64]. As Sather and McCleskey put it in their review [63] "The calcium channel field is convinced that the EEEE carboxyl side chains project into the pore lumen" to form a mixture of ions and side chains that has been called an 'electrical stew'[65].

At room temperature of 300K, these side chains as well as the surrounding cations interact and exhibit thermal motions. The four glutamates (EEEE) contribute to a fixed charge of -4*e* on the selectivity filter. This existing information about the L-type calcium channel is used to build a reduced model [55, 66].

In our reduced model the channel is represented as a doughnut-shaped object with a pore in the middle connecting the two baths (Fig. 1). The protein which forms the pore is represented as a continuum solid with dielectric coefficient, $\varepsilon_p = 10$. The central, cylindrical part of the pore, the selectivity filter, is assigned a radius $R = 3.5$ Å and length $H = 10$ Å. The model is rotationally symmetric along the pore axis. The selectivity filter (–5 Å, 5 Å) contains the negatively charged side chains extending from the polypeptide backbone of the channel protein into the pathway for ionic movement. We represent the carboxyl (COO^-) side chains as a pair of negative half charged oxygen ions ($O^{1/2-}$) resulting in 8 oxygen ions (also called 'structural ions'). The net charge in the selectivity filter therefore sums to -4*e*. The side chains are free to rearrange inside the selectivity filter of the channel but cannot leave the selectivity filter. The mobile ions (Na^+, Ca^{2+}, Cl^-) as well as the oxygen ions of the carboxyl groups are hard spheres and are assigned Pauling crystal radii (see caption of Figure 1). The structural ions mix with the mobile ions producing a flexible but confined environment in the selectivity filter. The structural ions have different degrees of flexibility as described later. Water is represented implicitly as a dielectric ($\varepsilon_w = 80$).

The simulation cell is a cylindrical compartment that is kept small to save computation

time. The simulation cell is checked to be sure that it is large enough that our final results do not depend on its size. The dimensions of the simulation cell are chosen depending on the ionic concentrations in the surrounding bath solutions. The baths are separated by a lipid membrane 20 Å thick except where the channel protein is found. Ions are excluded from the lipid membrane. The filter is assumed to have a dielectric coefficient of 80. If more realistic values were used, the amount of computation required for the electrostatics increased and no significant effects were noticed on the simulation results [66, 67].

Method: Equilibrium Grand Canonical Monte Carlo Simulations

We perform Monte Carlo (MC) simulations using Metropolis sampling in the grand canonical ensemble [68] which allows us to efficiently simulate the very small ionic concentrations important for calcium channels. The details of the methods of sampling and their acceptance tests have been described in [67-70] and earlier papers. We simulate an equilibrium grand canonical ensemble at room temperature 300K. The chemical potentials of ions are the inputs chosen for the grand canonical ensemble and are determined separately using an iterative method [71, 72]. The acceptance tests of new particle configurations involve the total electrostatic energy of a configuration. The net electrostatic energy of the system includes the Coulombic interactions between the ions and the side chains and the interactions resulting from the charges induced at dielectric boundaries which are computed using the induced charge computation method [73]. The GCMC simulations that we present in the results section are averages of many runs performed on multiple processors and beginning from different seed configurations. Each result is the average of 6×10^8 to 1.2×10^9 MC configurations.

Simulated Experimental Setup

The micromolar block of Na^+ current observed by McCleskey et al. [74, 75] is a characteristic behavior of the L-type calcium channel. In this experiment, $CaCl_2$ is gradually added to a fixed background of 30 mM NaCl. The experiments show that 1 μM of Ca^{2+} reduces the current through the L-type calcium channel to the half its value in the absence of Ca^{2+}. This result implies that the selectivity filter of the calcium channel contains a high affinity binding site for cations, especially for Ca^{2+}. The strongly bound Ca^{2+} obstructs the diffusion of Na^+ ions in the packed and narrow selectivity filter. This experiment was the main target of several theoretical and simulation studies of the L-type calcium channel[23, 54, 66, 67, 70, 76, 77].

As far as we know, our reduced model is the only one that is able to produce this strong Ca^{2+} vs. Na^{+} selectivity in a range of conditions. Indeed most computations of selectivity do not contain concentration as a variable at all [1, 2, 78]. Moreover, classical kinetic models of selectivity [79, 80] assume the energy landscape or the barrier to be independent of ionic concentrations which is an implausible approximation given the ubiquity of shielding in ionic solutions and the reality of Gauss' law. These and other difficulties with classical models have been evident for a long time [81-91]. Indeed, the 'law' of mass action itself has recently been shown to apply only to infinitely dilute solutions of noninteracting particles, if it is used with constant rate constants as in classical models of channels [79, 80].

Our simulations (analyzed with the integrated Nernst-Planck equation, see later eq. (3)) show that at 1 μM Ca^{2+} the average number of Na^{+} ions in the selectivity filter drops to half the value it has at zero Ca^{2+}. Under those conditions, Ca^{2+} ions occupy the central binding site in the filter, but they do not contribute to the current because of the depletion zones formed at the entrances of the filter [23, 77]. This mechanism is in agreement with an earlier intuitive description of the mechanism of this block [92].

Some simulations were carried out for the entire range of Ca^{2+} concentrations as used by Almers and McCleskey in their experiment (from zero to 10^{-2} M). Others were just carried out for the special case when $[Ca^{2+}]$ is 1μM. In experiments, the replacement of Na^{+} by Ca^{2+} takes place in a narrow concentration range around this value.

Models of Flexibility

There are two limiting cases of the flexibility of side chains.

(1) 'the flexible case' is our usual model with maximum flexibility. In this case, oxygen ions are perfectly mobile inside the selectivity filter but they are confined within the filter by hard walls. In this model, oxygen ions automatically find their average distribution that minimizes free energy of the system. As cations (Na^{+} or Ca^{2+}) enter the filter, oxygen ions rearrange and make it possible for the cations to pass the channel [56]. The distribution of the oxygens is an output of the simulation.

There is agreement [60, 61, 63, 93, 94] that side chains in the filter of calcium channels are quite flexible. They are in constant thermal motion and the long (3-carbon) chains allow the

COO^- end groups considerable freedom to move within the channel. Nonetheless, the maximum mobility case obviously overestimates the flexibility of side chains.

(2) the '*fixed*' case places oxygen ions in fixed positions and allows zero mobility. This assumption roughly corresponds to the system at 0 K and underestimates the flexibility of side chains.

Unfortunately, the X-ray structure for the calcium channel is not yet known. Therefore, instead of assuming the initial positions of the oxygens, we choose certain fixed oxygen configurations from the billions of possible configurations that are computed during an MC simulation of the '*flexible*' case. The nature of MC simulations ensures that all these configurations occur in the sample in a Boltzmann distribution[95, 96]. Each configuration we choose as a fixed configuration is one of the configurations of the equilibrated system. In other words, they can be called '*probable*' configurations.

In this paper, we chose configurations that are even 'more probable' using a criteria based on electrostatic energy. We determine those configurations by carrying out the usual MC simulation for 50 blocks where each block consists of 5×10^5 trials. After a block is finished, we displace the oxygen ions to ensure that the next block samples new configurations. After every MC trial in each block we calculate the electrostatic interaction energy of the oxygen ions with every other ion. A running average of this energy is updated. At the end of each block, the instantaneous locations of the oxygen ions and the corresponding running averages of the energy for that block are saved. Therefore, at the end of the simulation for each of the 50 blocks we obtain a set consisting of locations for the 8 oxygen ions which represent the instantaneous configurations at the end of the block and the corresponding average energy of that block. We have chosen 10 configurations of the oxygens from these 50 configurations that have the lowest average energy and we call them the '*low energy*' configurations. We have performed simulations for these cases in the usual way except that MC movements were not performed for the oxygen ions. We performed simulations for $[CaCl_2] = 10^{-6}$ M and $[CaCl_2] = 0$ M so we can relate our results for 10^{-6} M to results in the entire absence of Ca^{2+}.

In addition to these 10 '*fixed low energy*' configurations, we chose a configuration of oxygens that had the lowest energy in the sample we checked. This configuration does not have the lowest energy in general; it just has the lowest energy in the 50 configurations of oxygens we examined in our simulation. We will call this case the '*lowest energy*' case. We simulated the

lowest energy case for concentrations spanning the whole Ca^{2+} concentration range used in experiments.

Because we do not know the exact structure of the selectivity filter, the configurations just defined were not selected with the purpose to mimic any realistic structure. They were chosen to study the effect of fixing the oxygens somewhere. A large number—hundreds—of other configurations were chosen by *ad hoc* methods in the course of these calculations, as we developed our procedures. From all this work, we are quite certain that the conclusions that we draw from the results are quite general and independent of the actual positions of the oxygen ions. The qualitative conclusions of our work are not sensitive to the exact method of choosing the 'low energy' configurations. The exact configuration we call 'low energy' has little importance.

To study the effect of oxygen-flexibility in more detail, we constructed models in which oxygen ions have partial flexibility. These models lie between the fixed and flexible cases defined above.

(1) the '*restricted*' case restricts the 4 pairs of oxygen ions to stay in four narrow regions. We assume that the glutamate residues are not concentrated at one position of the selectivity filter, but rather they are distributed along the axis of the pore confined in cylinders defined by the filter wall and hard walls at fixed z-coordinates as shown in Fig. 2. The regions in which the oxygen-pairs are confined overlap and they prevent a given pair to diffuse elsewhere in the filter. The distribution of oxygen ions is more uniform in this case than in the '*flexible*' case. We performed simulations for this case in the whole Ca^{2+} concentration range where the oxygen ions were perfectly mobile in the selectivity filter $|z| \leq 3.6$Å.

(2) the 'confined' case. In this case, we start with the '*lowest energy fixed*' position of the oxygen ions and gradually allow them more and more mobility in the following way. We define spheres of radii R_{ox} around these fixed positions and allow the oxygen ions to move freely inside these spheres. The oxygen ions cannot leave these spheres. Then, we gradually increase the size of these spheres thus increasing the mobility of the oxygen ions. Any radius that is larger than 7.2 Å effectively corresponds to the '*flexible*' case. Thus, we designed a scheme in which we smoothly change the model between the two limiting cases of flexible and fixed. We performed simulations in the confined case only for $[CaCl_2] = 10^{-6}$ M and $[CaCl_2] = 0$ M.

Pore Conductance

We use the integrated Nernst-Planck formulation of Gillespie and Boda [77, 97] to relate the equilibrium GCMC simulation to the linearized slope conductance estimated in experiments with equal concentrations of ions on both sides of the channel. The integrated Nernst-Planck formulation based on the resistors-in-series model is used to calculate the conductance of each ionic species in the pore region. The combination of the integrated Nernst Planck equation (3) and MC simulations has been successful in reproducing the anomalous mole fraction effect in L-type calcium channel known from experiment [77]. We reproduce here the key equations that we use in our calculations.

The ions are assumed to move diffusively and their current is described by the Nernst Planck equation

$$-\mathbf{J}_i(\mathbf{x}) = \frac{1}{k_B T} D_i(\mathbf{x}) \rho_i(\mathbf{x}) \nabla \mu_i(\mathbf{x}), \tag{1}$$

where $\mathbf{J}_i(\mathbf{x}), D_i, \rho_i,$ and μ_i are the local flux density, diffusion coefficient, density and the electrochemical potential respectively of ion species i.The value k_B is the Boltzmann constant and T is the temperature. We focus on the selectivity filter region of length L and cross-sectional area $A(z)$ confining the structural ions. The chemical potential $\mu_i(z)$ and the diffusion coefficient $D_i(z)$ are assumed to be uniform over the cross-section of the selectivity filter. With these approximations, the total flux of ion species i through the pore:

$$-J_i^T = \frac{D_i}{k_B T} \frac{d\mu_i(z)}{dz} n_i(z), \tag{2}$$

where $n_i(z)$ is the axial number density of ions (number per unit pore length) at axial location z.

The total conductance γ of the pore in the presence of symmetrical bath solutions at the end of the selectivity filter region containing several ion species of charge $z_i e_0$ and a very small voltage applied across the system is:

$$\gamma = e_0 \sum_i z_i \frac{\partial J_i^T}{\partial V}\Big|_{V_{L/2} - V_{-L/2}} = \sum_i D_i \frac{z_i^2 e_0^2}{k_B T} \left(\int_{-L/2}^{L/2} \frac{dz}{n_i(z)} \right)^{-1}. \tag{3}$$

Note that the conductance depends on the square of the charge of the ions $z_i^2 e_0^2$. The axial densities of ion species n_i are computed from the MC simulations. The diffusion coefficient of ions is an external parameter not determined by our simulation that must be provided as an input to our computation. We deal with normalized conductances and therefore, it is sufficient to specify the ratio of diffusion coefficients of the two cations D_{Ca}/D_{Na}. We use the value $D_{Ca}/D_{Na}{}^{+} = 0.1$ in our computation. Dynamical Monte Carlo (DMC) simulation [56] recently verified an early suggestion of Nonner and Eisenberg [76] that the diffusion coefficient of Ca^{2+} in the selectivity filter is much smaller than that of Na^{+}.

The approximations and equations used to calculate the pore conductance γ quantifies the current through the channel. It is very important here to emphasize that the estimation of pore conductance requires only the spatial (i.e., cross sectional) uniformity of the chemical potential, which does not imply that the other variables, such as the spatial number density of the ions or the electrical potential are spatially uniform. The concentration profiles used in these calculations are obtained from simulations performed under equilibrium conditions and with self-consistent electrostatics. When the system is off equilibrium the concentration profiles will have to be recomputed to be self-consistent as done in Density Functional/Poisson Nernst Planck theory [77, 97-101] or more recently with variational methods[50, 51, 102]. Thus, our conductance γ of eq. (3) does not include the nonlinear effects that may occur when other voltages or concentration gradients are applied. The non-equilibrium effects on the potential profiles cannot be determined by the equations given here. Non-equilibrium effects are important in channels because channels are devices that use gradients of free energy to perform their function. Non-equilibrium effects are responsible, for example, for the properties of semiconductor devices and those effects are not present near equilibrium where our conductance equation applies. Such effects can be computed by Poisson Nernst Planck equations if charge carriers have zero diameter or by a modification of those equations if the charge carriers have finite diameter [50, 51, 99, 102-106]. The slope conductance γ is nonetheless quite informative, because experiments show that current-voltage curves are linear in wide voltage range around equilibrium.

RESULTS

We analyze our results on various levels of abstraction. The primary output of our simulations is concentration profiles. These profiles describe the probability of various ions being found in a given position, or, looking at the same thing from a more dynamical point of view, they describe the relative amount of time that these ions spend in a given location. We will show profiles averaged over the cross-section of the channel. We can derive two kinds of integrated quantities from the concentration profiles.

(1) The integral of the concentration profile provides the average number of the given ionic species in a certain sub-volume of the system. We will show average number of ions integrated over the selectivity filter and we will call these numbers occupancies. The occupancies of Na^+ and Ca^{2+} describe equilibrium binding affinity of these ions to the selectivity filter.

(2) The other integrated quantity of interest is the integral of the reciprocal of the concentration profile based on the Nernst-Planck equation (see Methods section, eq. (3)). This integral is proportional to the resistance of the pore to a given ionic species in the region of validity of the equation. We will show conductance values γ that are the reciprocals of the resistances. We will concentrate on conductances of Na^+, because Ca^{2+} does not conduct significant current in the conditions of interest, at micromolar [$CaCl_2$].

We work with normalized conductances. Usually, we normalize with respect to the Na^+ conductance computed in the absence of Ca^{2+}. Because in this paper we compare different systems, we have two choices regarding how we normalize the conductance.

(A) First, each model (‘*flexible*’, ‘*restricted*’, ‘*fixed*’ or ‘*constrained’* cases) can be normalized by its own zero-Ca^{2+} conductance. Each model is normalized by itself. In this way, *g* is always normalized to 1 in the limit [$CaCl_2$] $\rightarrow$ 0. This kind of normalization is used in the experimental literature [60, 61, 63, 74, 75, 94].

(B) To compare the absolute values of conductances computed from different models, we can normalize with respect to one fixed value in all cases. This way, we can draw conclusions about how changing the flexibility of the oxygen ions influences the ability of the channel to conduct Na^+. Correlations between the integrated quantities are shown by plotting one integrated quantity on the ordinate, and the other integrated quantity on the abscissa.

Fig. 3 shows concentration profiles for the (A) ‘*flexible*’, (B) ‘*restricted*’, (C) ‘*lowest energy fixed*’, and (D) the average of the 10 ‘*low energy fixed*’ cases. The oxygen concentration

profiles (top panels of Figs. 3A-D) are similar in the '*flexible*' and '*restricted*' cases: oxygen ions tend to accumulate at the entrances of the filter because the negative oxygen ions repel each other to the confining walls of their compartment. A third peak appears in the center of the filter in the '*flexible*' case because of packing. In the '*restricted*' case, the total oxygen profile is a sum of the four profiles for the four oxygen pairs. The '*restricted*' case has two additional peaks. The distribution of oxygens is more flat than in the '*flexible*' case. The vertical lines in the '*lowest energy fixed*' case represent Dirac-delta functionals describing the positions of the fixed oxygens.

Each simulation performed with a given fixed oxygen configuration provides an adequate sampling of all possible configurations of the free ions (Na^+, Ca^{2+}, and Cl^-), because of the large number of configurations calculated (and examined) in each simulation. Many of the configurations we have chosen for the fixed oxygens produce configurations of the free ions that resemble results of simulations of the totally '*flexible*' case. The 10 selected '*low energy fixed*' simulations then correspond to a sample that resembles a sample of the '*flexible*' case. The resemblance is approximate because we have only 10 '*low energy fixed*' oxygen configurations compared to the millions of oxygen configurations found in a usual simulation for the entire '*flexible*' case. (Remember the result of a Monte Carlo simulation is a set of configurations, not a single configuration.) To test this idea, we averaged the concentration profiles obtained from the 10 simulations for the 10 '*low energy fixed*' cases. The oxygen profile shown in the top panel of Fig. 3D was calculated using a wide (1 Å) bin. The overall behavior of the curve is very similar to the oxygen profile for the '*flexible*' case despite the small (10) sample for the oxygens in the '*low energy fixed*' case.

The bottom panels of Figs. 3A-D show the results for the free ions (Na^+ and Ca^{2+}) for $[CaCl_2] = 10^{-6}$ M and $[CaCl_2] = 0$ M. A micromolar amount of Ca^{2+} in the bath is sufficient to decrease the Na^+ concentration in the pore to the half of its value in the absence of Ca^{2+}. (Compare the thick solid and thin dashed lines.) From this point of view, the four models behave similarly. The similarity is especially striking in the case of the '*lowest energy fixed*' oxygen configuration: although the details of the distribution of Na^+ ions are very different from those in the '*flexible*' and '*restricted*' cases, the relative behavior with respect to the zero-Ca^{2+} curve is similar. This is also true for the average of the 10 '*low energy fixed*' cases.

This is the first important conclusion of our paper: adding Ca^{2+} to the systems simply scales the Na^{+} spatial profiles but it does not change the shape of the spatial distribution. Furthermore, adding 1 μM Ca^{2+} scales the Na^{+} profiles similarly in the three different cases, thus producing similar selectivity behavior. This scaling is shown by Fig. 4, where we plot the ratio of the Na^{+} concentration spatial profiles for $[CaCl_2] = 10^{-6}$ M and $[CaCl_2] = 0$ M. This ratio is similar for the three cases plotted showing that these three models have similar selectivity behavior. The 10 '*low energy fixed*' cases have the same behavior on average. The shape of the curves is very similar in the individual cases too (data not shown).

Ca^{2+} profiles also behave similarly in the various cases in this respect. As Ca^{2+} is added, it appears in the selectivity filter wherever space is available (at the minima of the oxygen profiles).The common feature is that Ca^{2+} is absent at the filter entrances ($3.0 \leq |z| \leq 5$Å).

Depletion zones—here at the filter entrances—have the property that the reciprocal of the Ca^{2+} concentration is large at these locations, so the integral (of the reciprocal of the concentration profile, which is the resistance) is also large. Various slices of the channel along the pore axis behave as resistors connected in series. One high-resistance element makes the resistance of the whole circuit high. Therefore, Ca^{2+} does not carry any current at this concentration; it only blocks (reduces) the current of Na^{+}.

Here we see the origin of the most noted experimental property of the calcium channel, calcium block. Calcium block of sodium current is produced by the selective binding of Ca^{2+} in the selectivity filter. The absence of calcium current (an important part of the block) is produced by depletion zones. The depletion zones are computed outputs of our model, not assumed inputs.

To describe further the selectivity behavior of the channel models using the integrated quantities, we show titration curves. We plot these integrated quantities as a function of the concentration of added Ca^{2+}.

Fig. 5A shows the occupancy curves for both Na^{+} and Ca^{2+}. Ca^{2+} gradually replaces Na^{+} in the filter as $[CaCl_2]$ increases. At about 1 μM, the two ions have equal amount in the filter. Also, at this Ca^{2+} concentration the amount of Na^{+} drops to half in the filter. The three different cases behave similarly in spite of the differences in fine details in the concentration profiles (see Fig. 3).

Fig. 5B shows the normalized Na^{+} conductances (normalized by their own zero-Ca^{2+} values) for the three different cases. The current carried by Na^{+} is gradually decreased as Ca^{2+} is

added in accordance with the experiment of Almers and McCleskey [74, 75]. As we demonstrated before, we reproduce the micromolar block of the current by Ca^{2+}, our curves agree well with the experimental curve in the low [$CaCl_2$] range. Ca^{2+} starts to conduct at high [$CaCl_2$]. In this regime, our agreement with experiments is only qualitative due to differences between the theoretical and experimental situations as described previously [77]. (In experiments, Ca^{2+} is added only to the extracellular side, while our setup is symmetrical.) Note that the occupancy and conductance curves for Na^+ behave similarly indicating a strong correlation between these two quantities (see later discussion).

Fig. 6 shows the correlation between Na^+ conductance and Na^+ occupancy. The correlation was evident from Fig. 5, but this figure shows it clearly: the more Na^+ we have in the filter, the larger the pore's conductance for Na^+. Again, the various '*fixed*' oxygen points scatter over a relatively wide range, but this figure clearly shows that the large drop in both occupancy and conductance occurs in a relatively narrow concentration range around 1 μM. In the range of lower and higher [$CaCl_2$] (below and above 10^{-6} M), the values do not change very much. Also, the average of the 10 '*low energy fixed*' cases is quite close the '*flexible*' and '*restricted*' cases that allow (some) movement of the oxygens.

In the previous figures, conductances were normalized by the conductances obtained at zero Ca^{2+} for a given case. Fig. 7 was designed to show correlation between the conductances normalized in the two different ways described previously, if correlations existed. No correlations were found. Normalization of results from a model by the zero Ca^{2+} conductance of that model shows the selectivity of that model. The lower this normalized value (shown on the abscissa), the more selective the model is for Ca^{2+}. On the other hand, if we normalize by one specific value—the zero Ca^{2+} conductance for the '*flexible*' case—we can tell how the conductance of the model for Na^+ changes as we change the flexibility of the oxygen ions. The lack of correlation indicates that a given *fixed* oxygen configuration can favor selectivity and conductance independently. Conductance is sensitive to the presence of depletion zones, while selectivity is more sensitive to the degree of competition between Ca^{2+} and Na^+.

The relative conductance in comparisons between different models depends primarily on the oxygen configuration. A configuration can be 'fortunate' (large conductance) so that Na^+ ions find enough space between the crowding oxygen ions. A configuration could also be 'unfortunate', meaning that the oxygen ions are in positions that act as obstacles for the passing

Na^+ ions and produce deep depletion zones for them. Indeed, sometimes the location of oxygens create depletion zones where Na^+ concentration is zero, so the conductance is also zero. The '*flexible*' and '*restricted*' cases are statistical averages of the many '*fixed*' configurations in some sense or other. Therefore, these averaged cases do not suffer from the unfortunate configurations found in individual unaveraged cases: there are always enough configurations in the sample in the averaged cases in which oxygen ions move away and give way to the Na^+ ions. The average of the 10 '*low energy fixed*' cases is another example where the fortunate cases balance the unfortunate cases. Another interesting result shown in the figure is that the conductance of the '*restricted*' model is larger than that of the '*flexible*' model. The conductance is larger because the distribution of Na^+ ions is more spatially uniform for this model (see Fig. 2). Therefore, the depletion zones of Na^+ are less deep in this case.

Fig. 8 shows the concentration profiles for $O^{-1/2}$, Na^+, and Ca^{2+} for our other model with different oxygen flexibility. When the oxygen ions are fixed (R_{ox} = 0 Å), the Na^+ and Ca^{2+} ions have high peaks in the regions where oxygen ions are absent. As the R_{ox} is increased, the peaks become lower, the valleys become less deep, and the curves eventually converge to those of the '*flexible*' model.

Fig. 9 shows the conductance and occupancy of Na^+ as a function of R_{ox}. The conductances are normalized by the value at R_{ox} = 0 Å. There are two maxima in the conductance. It seems that conductance is larger in a model that is not perfectly '*flexible*', but not perfectly '*fixed*' either. In the '*fixed*' model, the oxygen ions act as obstacles as described above, especially if their configuration is 'unlucky'. In the '*flexible*' case, the oxygen ions act as obstacles because they pile up at the filter entrances thus producing depletion zones for the Na^+ ions.

There is a clear correlation between conductance and occupancy: less Na^+ means more Na^+-conductance. Intuitively, we might expect the opposite. The explanation is that although we have less Na^+ (smaller peaks), as R_{ox} is increased, we also—in the same profile—have shallower depletion zones (see Fig. 8).

DISCUSSION

Some Flexibility of Side Chains is Required for Calcium Selectivity

We investigated the role of flexibility by comparing differential quantities and integral quantities in the selectivity filter of the 'flexible', 'fixed' and 'restricted' models. We compared the differential quantities, the distribution of the side chains (oxygens) and the cations (Na^+ and Ca^{2+}) and the integrated quantities, the occupancies of cations Ca^{2+}/ Na^+ and linearized conductance of Na^+.

The differential quantities that we obtain from our model show a strong dependence on the locations of fixed side chains and the flexibility of the side chains. We show that holding the side chains fixed at certain predetermined locations in the selectivity filter distorts the distribution of Ca^{2+} and Na^+ in the selectivity filter. This distortion can result in a loss in selectivity because the distribution of the cations is determined by the distribution of the side chains (Figure 3C). This reasoning is further supported (1) by calculations (Fig. 8) which vary the mobility of the side chains in the radial direction from frozen to perfectly mobile and (2) by calculations (Figures 3, A and B) of the 'restricted model' in which the side chains are allowed to have a limited flexibility along the channel axis. The results are similar to the usual 'flexible' case.

However, the behavior described by the integrated quantities (occupancy and normalized conductance) is much less sensitive, as might be expected from averaged, i.e., integrated quantities which are, as a rule, much less sensitive than differential quantities. Behavior of integrated quantities is similar in the 'restricted', 'fixed', and 'flexible' models. The occupancy of Ca^{2+} increases with the increasing bath concentration of Ca^{2+} (while occupancy of Na^+ decreasing) and the normalized conductance of Na^+ is reduced with increasing amount of Ca^{2+} in bath. Thus, the integrated quantities obtained from our model are much less sensitive to details of structure. They do not show sensitivity to the flexibility and the locations of the side chains.

Our results show that some flexibility of side chains is necessary to avoid obstruction of the ionic pathway by oxygen ions in 'unlucky' fixed positions. When oxygen ions are mobile, they adjust 'automatically' to accommodate to the permeable cations in the selectivity filter.

Beyond the rigid (fixed oxygen) case, however, our results seem quite insensitive to how and what degree do we make the side chains flexible. Density profiles and selectivity (expressed

in term of either occupancy or conductance) behave similarly in the different models of flexibility ("flexible", "restricted", and "confined").

The exact location and mobility of oxygen ions (let alone even finer details of structure) have little effect on the selectivity behavior of calcium channels. Seemingly, nature has chosen a robust mechanism to control selectivity in calcium channels: the first order determinant of selectivity is the volume of the selectivity filter with the charge and excluded volume of structural ions confined within it. Flexibility of side chains seem to belong to the group of second order determinants. These conclusions of course apply to what we study here. Flexibility and fine structural details may have important role in other properties of calcium channels that are not studied in this paper.

These results justify our early assumption—suggested by Nonner et al. [55] using theory and further studied with MC simulations [54, 66, 107]—that the important factor in Ca^{2+} vs Na^{+} selectivity is the density of oxygen ions in the selectivity filter. Later studies (41,42) showed the importance of (charge) polarization (i.e., dielectric properties). The assumption of maximum mobility of oxygens (‘flexible’ case), seems to be an excellent approximate working hypothesis in the absence of exact structural information. We look forward to seeing how well the real structure fits within this hypothesis, when it becomes available.

Self-organized Induced Fit Model of Selectivity

Our results from the simulations of the zero flexibility model and the restricted flexibility model suggest that the reduced model is actually an induced fit model of selectivity, a specific version of the induced fit model of enzymes [108] in which biological function is controlled by the flexibility of the side chains that allows the side chains to self-organize into structures that change with changing ionic conditions.

The variation of binding with concentration and type of ions arise from different structures that self-organize under different ionic conditions. The fit of the protein side chains to the ions, and the fit of the ions to the protein, change with conditions. The different fit in different types of ions produces selectivity. The structures—in the sense defined in this paper—vary with concentration as well as type of ion. The energy of the structures varies with concentration and type of ion and we know of no simple theory to calculate this change in energy. Simulations are needed in a range of concentrations and types of solutions. Calculations that characterize selectivity by a single free energy of binding do not address these issues. They

also do not address the issue of how selectivity occurs in life or in experiments in which ions appear in mixed solutions of varying concentration.

Induced fit and self-organized models have traditionally been focused on the average structure of the protein. Here we view the locations of ions as part of the structure and we find that the distribution of locations ('flexibility', 'entropy') is also important. Monte Carlo methods used by Boda et al. [69, 70, 77, 107, 109, 110] seem ideally suited to make the qualitative idea of self-organized systems and induced fit of enzymes into a quantitatively specific (and testable) hypothesis of protein function. The self-organized/induced fit theory says that all relevant atoms are in an equilibrium distribution of positions and (perhaps) velocities. Monte Carlo methods are used to estimate such distributions in many areas of physics. These methods seem to be less sensitive to sampling errors than traditional forms of molecular dynamics for many reasons discussed at length in the literature [111, 112].

Selectivity in these channels arises from the interaction of the flexible side chains with the ions. The balance of the two main competing forces—electrostatic and excluded volume—in the crowded selectivity filter of the reduced model determines the binding site for Ca^{2+}. The structure of the binding site is an output of the calculations which rearranges according to the surrounding ionic conditions. The word 'structure' is somewhat inadequate to describe what is happening here. The thermal motions of the structure are as important as the average location. The biologically important properties depend on the entire ensemble of trajectories of ions and side chains. The distributions of location and velocities are involved. Traditional self-organized/induced fit models need to be generalized to include the self-organized/induced entropy (i.e., flexibility) as well as the self-organized/induced energy (i.e., location).

The success of the self-organized induced fit model of selectivity arises because it calculates structures instead of assuming them. Assuming a preformed structure, independent of conditions, distorts the model significantly. Evidently, assuming a constant structure involves applying an artificial constraint not present in real channels. We suspect, but have not proven, that the difficulty is fundamentally similar to that which arises when a protein is described by a potential surface independent of conditions instead of as a distribution of permanent and dielectric charge [87, 88].

Monte Carlo methods developed by Boda et al. seem ideally suited to compute the equilibrium properties of these self-organized systems. Other methods are needed to extend to

the general non-equilibrium conditions in which most channels and proteins function, for example, variational methods like *EnVarA* [105, 106] or PNP-DFT [99, 103, 104].

ACKNOWLEDGEMENTS

We thank our colleague and friend Prof. Eduardo Rios for suggesting the name "*flexible confinement*". We are grateful for a generous allotment of computing time at the MARYLOU supercomputing facility of Brigham Young University. Discussions with Wolfgang Nonner and Dirk Gillespie were most valuable and welcome. The work was supported in part by NIH grant GM076013. Dezső Boda acknowledges the support of the Hungarian National Research Fund (OTKA K75132).

REFERENCES

1. Roux, B. 2010. Perspectives on: Molecular dynamics and computational methods. Journal of General Physiology 135:547-548.

2. Roux, B. 2010. Exploring the Ion Selectivity Properties of a Large Number of Simplified Binding Site Models. Biophysical Journal 98:2877-2885.

3. Hagiwara, S., and K. I. Naka. 1964. The Initiation of Spike Potential in Barnacle Muscle Fibers under Low Intracellular Ca++. J Gen Physiol 48:141-162.

4. Gerasimov, V. D., P. G. Kostyuk, and V. A. Maiskii. 1965. Action potential production in giant neurons of mollusks. Fed Proc Transl Suppl 24:763-767.

5. Kostyuk, P. G., O. A. Krishtal, V. I. Pidoplichko, and N. S. Veselovsky. 1978. Ionic currents in the neuroblastoma cell membrane. Neuroscience 3:327-332.

6. Hagiwara, S. 1979. Differentiation of Na and Ca channels during early development. Society of General Physiologists series 33:189-197.

7. Byerly, L., and S. Hagiwara. 1982. Calcium currents in internally perfused nerve cell bodies of Limnea stagnalis. J Physiol 322:503-528.

8. Hagiwara, S., and H. Ohmori. 1982. Studies of calcium channels in rat clonal pituitary cells with patch electrode voltage clamp. J Physiol 331:231-252.

9. Almers, W., and E. W. McCleskey. 1984. Non-selective conductance in calcium channels of frog muscle: calcium selectivity in a single-file pore. J.Physiol. 353:585-608.

10. Hagiwara, S., and K. Kawa. 1984. Calcium and potassium currents in spermatogenic cells dissociated from rat seminiferous tubules. J Physiol 356:135-149.

11. Lee, K. S., and R. W. Tsien. 1984. High selectivity of calcium channels as determined by reversal potential measurements in single dialyzed heart cells of the guinea pig. Journal of Physiology (London) 354:253-272.

12. Tsien, R. W., P. Hess, E. W. McCleskey, and R. L. Rosenberg. 1987. Calcium channels: mechanisms of selectivity, permeation, and block. Annual review of biophysics and biophysical chemistry 16:265-290.

13. Kostyuk, P. G. 1989. Diversity of calcium ion channels in cellular membranes. Neuroscience 28:253-261.

14. Corvalan, V., R. Cole, J. de Vellis, and S. Hagiwara. 1990. Neuronal modulation of calcium channel activity in cultured rat astrocytes. Proceedings of the National Academy of Sciences of the United States of America 87:4345-4348.

15. Yamashita, N., S. Ciani, and S. Hagiwara. 1990. Effects of internal Na+ on the Ca channel outward current in mouse neoplastic B lymphocytes. J Gen Physiol 96:559-579.

16. Kostyuk, P., and A. Verkhratsky. 1994. Calcium stores in neurons and glia. Neuroscience 63:381-404.

17. McCleskey, E. W. 1994. Calcium channels: cellular roles and molecular mechanisms. Current opinion in neurobiology 4:304-312.

18. Kirischuk, S., N. Voitenko, P. Kostyuk, and A. Verkhratsky. 1996. Calcium signalling in granule neurones studied in cerebellar slices. Cell calcium 19:59-71.

19. Zhang, J. F., P. T. Ellinor, R. W. Aldrich, and R. W. Tsien. 1996. Multiple structural elements in voltage-dependent Ca2+ channels support their inhibition by G proteins. Neuron 17:991-1003.

20. Rodríguez-Contreras, A., and E. N. Yamoah. 2003. Effects of Permeant Ion Concentrations on the Gating of L-Type Ca2+ Channels in Hair Cells. Biophysical Journal 84:3457-3469.

21. Gordon, S. E. 2010. Perspectives on: Local calcium signaling. The Journal of General Physiology 136:117.

22. Boda, D., W. Nonner, M. Valisko, D. Henderson, B. Eisenberg, and D. Gillespie. 2007. Steric selectivity in Na channels arising from protein polarization and mobile side chains. Biophys J 93:1960-1980.

23. Boda, D., M. Valisko, D. Henderson, B. Eisenberg, D. Gillespie, and W. Nonner. 2009. Ionic selectivity in L-type calcium channels by electrostatics and hard-core repulsion. J Gen Physiol 133:497-509.

24. Rahin, A. A., and B. Honig. 1985. Reevaluation of the Born model of ion hydration. J.Phys.Chem. B 89:5588-5593.

25. Gilson, M. K., and B. Honig. 1985. The dielectric constant of a folded protein. Biopolymers 25:2097-2119.

26. Warshel, A., and S. T. Russell. 1984. Calculations of electrostatic interactions in biological systems and in solutions. Quarterly Review of Biophysics 17:283-422.

27. Russell, S. T., and A. Warshel. 1985. Calculations of electrostatic energies in proteins. The energetics of ionized groups in bovine pancreatic trypsin inhibitor. Journal of molecular biology 185:389-404.

28. Head-Gordon, T., and C. L. Brooks. 1987. The role of electostatics in the binding of small ligands to enzymes. J Phys Chem B 91:3342-3349.

29. Gilson, M. K., and B. Honig. 1988. Calculation of the total electrostatic energy of a macromolecular system: solvation energies, binding energies, and conformational analysis. Proteins 4:7-18.

30. Gilson, M. K., K. A. Sharp, and B. H. Honig. 1988. Calculating the Electrostatic Potential of Molecules in Solution: Method and Error Assessment. Journal of computational chemistry 9:327-335.

31. Honig, B., K. Sharp, and M. Gilson. 1989. Electrostatic interactions in proteins. Progress in clinical and biological research 289:65-74.

32. Davis, M. E., and J. A. McCammon. 1990. Electrostatics in biomolecular structure and dynamics. Chem. Rev. 90:509–521.

33. Sharp, K., A. Jean- Charles, and B. Honig. 1992. A local dilectric constant model for solvation free energies which accounts for solute polarizability. J Phys Chem B 96:3822-3828.

34. Honig, B., and K. Sharp. 1993. Macroscopic models of aqueous solutions: biological and chemical applications. Journal of Physical Chemistry 97:1101-1109.

35. Gilson, M. K. 1995. Theory of electrostatic interactions in macromolecules. Current opinion in structural biology 5:216-223.

36. Honig, B., and A. Nichols. 1995. Classical electrostatics in biology and chemistry. Science 268:1144-1149.

37. Antosiewicz, J., J. A. McCammon, and M. K. Gilson. 1996. The determinants of pKas in proteins. Biochemistry 35:7819-7833.

38. Simonson, T., and C. L. Brooks. 1996. Charge Screening and the Dielectric Constant of Proteins: Insights from Molecular Dynamics. Journal of the American Chemical Society 118:8452-8458.

39. Warshel, A. 1998. Electrostatic origin of the catalytic power of enzymes and the role of preorganized active sites. The Journal of biological chemistry 273:27035-27038.

40. Dominy, B. N., and C. L. Brooks. 1999. Development of Generalized Born Model Parameterization for Proteins and Nucleic Acids. J Phys Chem B 103:3675-3773.

41. Roux, B. 2001. Implicit solvent models. In Computational Biophysics. O. Becker, A. D. MacKerrel, R. B., and M. Watanabe, editors. Marcel Dekker Inc, New York. p. 133-155.

42. Schutz, C. N., and A. Warshel. 2001. What are the dielectric "constants" of proteins and how to validate electrostatic models? Proteins 44:400-417.

43. Baker, N. A., and J. A. McCammon. 2003. Electrostatic interactions. Methods of biochemical analysis 44:427-440.

44. Im, W., M. S. Lee, and C. L. Brooks III. 2003. Generalized Born Model With A Simple Smoothing Function. J Comput Chem 12:1894-1901.

45. Nielsen, J. E., and J. A. McCammon. 2003. Calculating pKa values in enzyme active sites. Protein Sci 12:1894-1901.

46. Swanson, J. M., J. Mongan, and J. A. McCammon. 2005. Limitations of atom-centered dielectric functions in implicit solvent models. J Phys Chem B Condens Matter Mater Surf Interfaces Biophys 109:14769-14772.

47. Zhu, J., E. Alexov, and B. Honig. 2005. Comparative Study of Generalized Born Models: Born Raddi and Peptide Folding. J Phys Chem B 109:3008-3022.

48. Dzubiella, J., J. M. Swanson, and J. A. McCammon. 2006. Coupling hydrophobicity, dispersion, and electrostatics in continuum solvent models. Phys Rev Lett 96:087802.

49. Henderson, D. 2009. Attractive Energy and Entropy or Particle Size: the Yin and Yang of Physical and Biological Science. Interdisciplinary Sciences: Computational Life Sciences 1:1-11 available on arXiv http://arxiv.org/ with PaperID 0901.3641.

50. Hyon, Y., B. Eisenberg, and C. Liu. 2010. A mathematical model for the hard sphere repulsion in ionic solutions. Preprint# 2318 of the reprint series of the Institute for Mathematics and its Applications (IMA, University of Minnesota, Minneapolis) http://www.ima.umn.edu/preprints/jun2010/jun2010.html.

51. Eisenberg, B., Y. Hyon, and C. Liu. 2010. Energy Variational Analysis EnVarA of Ions in Water and Channels: Field Theory for Primitive Models of Complex Ionic Fluids. Preprint# 2317 of the reprint series of the Institute for Mathematics and its Applications (IMA, University of Minnesota, Minneapolis) http://www.ima.umn.edu/preprints/jun2010/jun2010.html.

52. Barreiro, G., C. R. Guimaraes, and R. B. de Alencastro. 2002. A molecular dynamics study of an L-type calcium channel model. Protein Eng 15:109-122.

53. Lipkind, G. M., and H. A. Fozzard. 2001. Modeling of the outer vestibule and selectivity filter of the L-type Ca2+ channel. Biochemistry 40:6786-6794.

54. Malasics, A., D. Gillespie, W. Nonner, D. Henderson, B. Eisenberg, and D. Boda. 2009. Protein structure and ionic selectivity in calcium channels: Selectivity filter size, not shape, matters. Biochim Biophys Acta.

55. Nonner, W., L. Catacuzzeno, and B. Eisenberg. 2000. Binding and Selectivity in L-type Ca Channels: a Mean Spherical Approximation. Biophysical Journal 79:1976-1992.

56. Rutkai, G., D. Boda, and T. Kristof. 2010. Relating binding affinity to dynamical selectivity from dynamic Monte Carlo simulations of a model calcium channel. J.Phys.Chem.Lett. 1:2179-2184.

57. Markowich, P. A., C. A. Ringhofer, and C. Schmeiser. 1990. Semiconductor Equations. New York, Prentice Hall.

58. Shur, M. 1990. Physics of Semiconductor Devices. Prentice Hall, New York.

59. Eisenberg, B. 2005. Living Transistors: a Physicist's View of Ion Channels (version 2). http://arxiv.org/ q-bio.BM: arXiv:q-bio/0506016v2

60. Yang, J., P. T. Ellinor, W. A. Sather, J. F. Zhang, and R. Tsien. 1993. Molecular determinants of Ca2+ selectivity and ion permeation in L-type Ca2+ channels. Nature 366:158-161.

61. Ellinor, P. T., J. Yang, W. A. Sather, J.-F. Zhang, and R. Tsien. 1995. Ca2+ channel selectivity at a single locus for high-affinity Ca2+ interactions. Neuron 15:1121-1132.

62. Wu, X. S., H. D. Edwards, and W. A. Sather. 2000. Side chain orientation in the selectivity filter of a voltage-gated Ca2+ channel. J.Biol.Chem. 275:31778-31785.

63. Sather, W. A., and E. W. McCleskey. 2003. Permeation and selectivity in calcium channels. Annual review of physiology 65:133-159.

64. Koch, S. E., Ilona B., Arnold S. , and G. V. 2000. Architecture of Ca2+ Channel Pore-lining Segments Revealed by Covalent Modification of Substituted Cysteines. Journal of Biological Chemistry.

65. McCleskey, E. W. 2000. Ion channel selectivity using an electric stew. Biophys J 79:1691-1692.

66. Boda, D., M. Valisko, B. Eisenberg, W. Nonner, D. Henderson, and D. Gillespie. 2007. Combined effect of pore radius and protein dielectric coefficient on the selectivity of a calcium channel. Phys Rev Lett 98:168102.

67. Boda, D., M. Valisko, B. Eisenberg, W. Nonner, D. Henderson, and D. Gillespie. 2006. The effect of protein dielectric coefficient on the ionic selectivity of a calcium channel. J Chem Phys 125:34901.

68. Valleau, J. P., and L. K. Cohen. 1980. Primitive model electrolytes. I. Grand canonical Monte Carlo computations. The Journal of chemical physics 72:5935-5941.

69. Boda, D., D. Henderson, and D. Busath. 2002. Monte Carlo study of the selectivity of calcium channels: improved geometrical mode. Molecular Physics 100:2361-2368.

70. Boda, D., W. Nonner, D. Henderson, B. Eisenberg, and D. Gillespie. 2008. Volume exclusion in calcium selective channels. Biophys J 94:3486-3496.

71. Malasics, A., D. Gillespie, and D. Boda. 2008. Simulating prescribed particle densities in the grand canonical ensemble using iterative algorithms. Journal of Chemical Physics 128:124102.

72. Malasics, A., and D. Boda. 2010. An efficient iterative grand canonical Monte Carlo algorithm to determine individual ionic chemical potentials in electrolytes. J. Chem. Phys. 132:244103.

73. Boda, D., D. Gillespie, W. Nonner, D. Henderson, and B. Eisenberg. 2004. Computing induced charges in inhomogeneous dielectric media: application in a Monte Carlo simulation of complex ionic systems. Phys Rev E Stat Nonlin Soft Matter Phys 69:046702.

74. Almers, W., E. W. McCleskey, and P. T. Palade. 1984. Non-selective cation conductance in frog muscle membrane blocked by micromolar external calcium ions. J. Physiol. 353:565-583.

75. Almers, W., and E. W. McCleskey. 1984. Non-Selective conductance in calcium channels of frog muscle: calcium selectivity in a single-file pore. J.Physiol. 353:585-608.

76. Nonner, W., and B. Eisenberg. 1998. Ion Permeation and Glutamate Residues Linked by Poisson-Nernst-Planck Theory in L-type Calcium Channels. Biophys. J. 75: 1287-1305.

77. Gillespie, D., and D. Boda. 2008. The Anomalous Mole Fraction Effect in Calcium Channels: A Measure of Preferential Selectivity. Biophys. J. 95:2658-2672.

78. Varma, S., D. Sabo, and S. B. Rempe. 2008. K+/Na+ selectivity in K channels and valinomycin: over-coordination versus cavity-size constraints. Journal of molecular biology 376:13-22.

79. Hille, B. 1975. Ionic Selectivity, saturation, and block in sodium channels. A four barrier model. J Gen Physiol. 66:535-560.

80. Hille, B. 2001. Ionic Channels of Excitable Membranes. Sinauer Associates Inc., Sunderland.

81. Cooper, K., E. Jakobsson, and P. Wolynes. 1985. The theory of ion transport through membrane channels. Progress in Biophysics and Molecular Biology 46:51–96.

82. Hänggi, P., P. Talkner, and M. Borokovec. 1990. Reaction-rate theory: fifty years after Kramers. Reviews of Modern Physics 62: 251-341.

83. Fleming, G., and P. Hänggi. 1993. Activated Barrier Crossing: applications in physics, chemistry and biology. World Scientific, River Edge, New Jersey.

84. Cooper, K. E., P. Y. Gates, and R. S. Eisenberg. 1988. Surmounting barriers in ionic channels. Quarterly Review of Biophysics 21: 331–364.

85. Cooper, K. E., P. Y. Gates, and R. S. Eisenberg. 1988. Diffusion theory and discrete rate constants in ion permeation. J. Membr. Biol. 109:95–105.

86. Eisenberg, R. S., M. M. Klosek, and Z. Schuss. 1995. Diffusion as a chemical reaction: Stochastic trajectories between fixed concentrations. J. Chem. Phys. 102:1767–1780.

87. Eisenberg, R. S. 1996. Computing the field in proteins and channels. J. Membrane Biol. 150:1–25. Also available on http:\\arxiv.org as Paper arXiv 1009.2857v1001.

88. Eisenberg, R. S. 1996. Atomic Biology, Electrostatics and Ionic Channels. In New Developments and Theoretical Studies of Proteins. R. Elber, editor. World Scientific, Philadelphia. 269-357. Published in the Physics ArXiv as arXiv:0807.0715.

89. Chen, D., L. Xu, A. Tripathy, G. Meissner, and R. Eisenberg. 1997. Rate Constants in Channology. Biophys. J. 73:1349-1354.

90. Eisenberg, R. S. 1999. From Structure to Function in Open Ionic Channels. Journal of Membrane Biology 171:1-24.

91. Eisenberg, B. 2000. Permeation as a Diffusion Process. In Biophysics Textbook On Line "Channels, Receptors, and Transporters" http://www.biophysics.org/btol/channel.html#5. L. J. DeFelice, editor. Published in ArXiv as arXiv:0807.0721.

92. Dang, T. X., and E. W. McCleskey. 1998. Ion channel selectivity through stepwise changes in binding affinity. J Gen Physiol 111:185-193.

93. Wu XS, E. H., and Sather WA. 2000. Side chain orientation in the selectivity filter of a voltage-gated Ca2+ channel. J.Biol.Chem. 275:31778-31785.

94. Cibulsky, S. M., and W. A. Sather. 2000. The EEEE locus is the sole high-affinity Ca2+ binding structure in the pore of a voltage-gated Ca2+ channel: block by Ca2+ entering from the intracellular pore entrance. . Journal of General Physiology 116:349-362.

95. Gubernatis, J. E., editor. 2003. The Monte Carlo Method in the Physical Sciences, Celebrating the 50th Anniversary of the Metropolis Algorithm. American Institute of Physics, Melville, NY.

96. Christian, P. R., and G. Casella. 2004. Monte Carlo Statistical Methods

97. Gillespie, D., D. Boda, Y. He, P. Apel, and Z. S. Siwy. 2008. Synthetic Nanopores as a Test Case for Ion Channel Theories: The Anomalous Mole Fraction Effect without Single Filing. Biophys. J. 95:609-619.

98. Gillespie, D., W. Nonner, and R. S. Eisenberg. 2002. Coupling Poisson-Nernst-Planck and Density Functional Theory to Calculate Ion Flux. Journal of Physics (Condensed Matter) 14:12129-12145.

99. Gillespie, D. 2008. Energetics of divalent selectivity in a calcium channel: the ryanodine receptor case study. Biophys J 94:1169-1184.

100. Gillespie, D., J. Giri, and M. Fill. 2009. Reinterpreting the Anomalous Mole Fraction Effect. The ryanodine receptor case study. Biophyiscal Journal 97:pp. 2212 - 2221

101. Gillespie, D. 2010. Analytic Theory for Dilute Colloids in a Charged Slit. The Journal of Physical Chemistry B 114:4302-4309.

102. Eisenberg, B. 2010. Crowded Charges in Ion Channels. Advances in Chemical Physics (in the press) also available at http:\\arix.org as Paper arXiv 1009.1786v1

103. Gillespie, D., M. Valisko, and D. Boda. 2005. Density functional theory of the electrical double layer: the RFD functional. Journal of Physics: Condensed Matter 17:6609-6626.

104. Gillespie, D., L. Xu, Y. Wang, and G. Meissner. 2005. (De)constructing the Ryanodine Receptor: modeling ion permeation and selectivity of the calcium release channel. Journal of Physical Chemistry 109:15598-15610.

105. Eisenberg, B., Y. Hyon, and C. Liu. 2010. Energy Variational Analysis EnVarA of Ions in Water and Channels: Field Theory for Primitive Models of Complex Ionic Fluids. Preprint# 2317 of the reprint series of the Institute for Mathematics and its Applications (IMA, University of Minnesota, Minneapolis) http://www.ima.umn.edu/preprints/jun2010/jun2010.html.

106. Hyon, Y., B. Eisenberg, and C. Liu. 2010. A mathematical model for the hard sphere repulsion in ionic solutions Preprint# 2318 of the reprint series of the Institute for Mathematics and its Applications (IMA, University of Minnesota, Minneapolis) http://www.ima.umn.edu/preprints/jun2010/jun2010.html.

107. Boda, D., D. Henderson, and D. D. Busath. 2001. Monte Carlo Study of the Effect of Ion and Channel Size on the Selectivity of a Model Calcium Channel. Journal of Physical Chemistry B 105:11574-11577.

108. Koshland, D. 1958. Application of a Theory of Enzyme Specificity to Protein Synthesis. Proc. Natl. Acad. Sci. 44:98–104.

109. Boda, D., D. D. Busath, D. Henderson, and S. Sokolowski. 2000. Monte Carlo Simulations of the Mechanism of Channel Selectivity: the competition between Volume Exclusion and Charge Neutrality. Journal of Physical Chemistry B *104*:8903-8910.

110. Boda, D., D. Busath, B. Eisenberg, D. Henderson, and W. Nonner. 2002. Monte Carlo simulations of ion selectivity in a biological Na+ channel: charge-space competition. Physical Chemistry Chemical Physics (PCCP) 4:5154-5160.

111. Kokubo, H., J. Rosgen, D. W. Bolen, and B. M. Pettitt. 2007. Molecular Basis of the Apparent Near Ideality of Urea Solutions. Biophys. J. 93:3392-3407.

112. Yu, H., and B. Roux. 2009. On the utilization of energy minimization to the study of ion selectivity. Biophys J 97:L15-17.

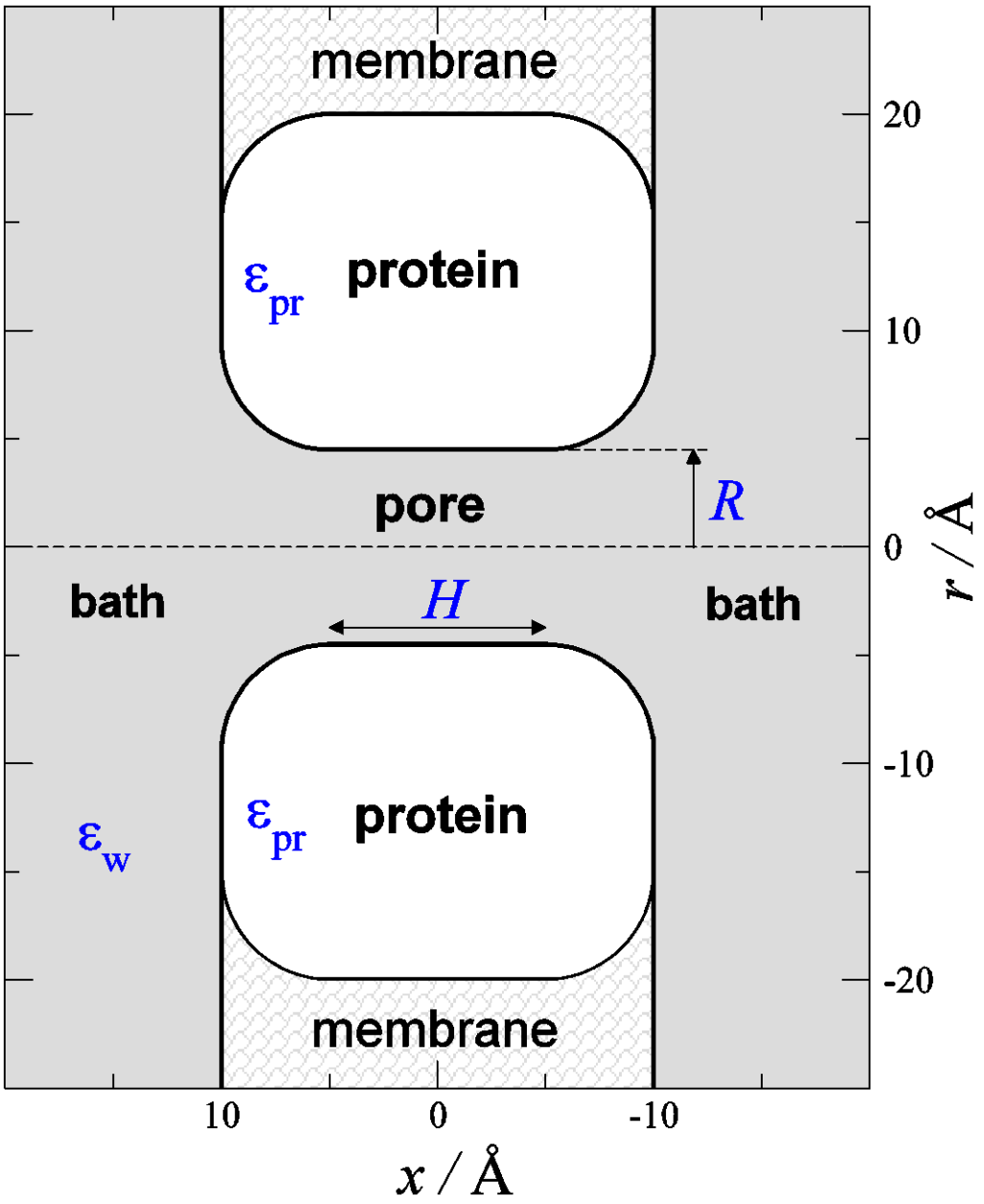

Fig. 1: Geometry of the model of the ion channel. The parameters R = 3.5 Å, H = 10 Å, and ε_{pr} = 10 are used in the simulations in this paper.

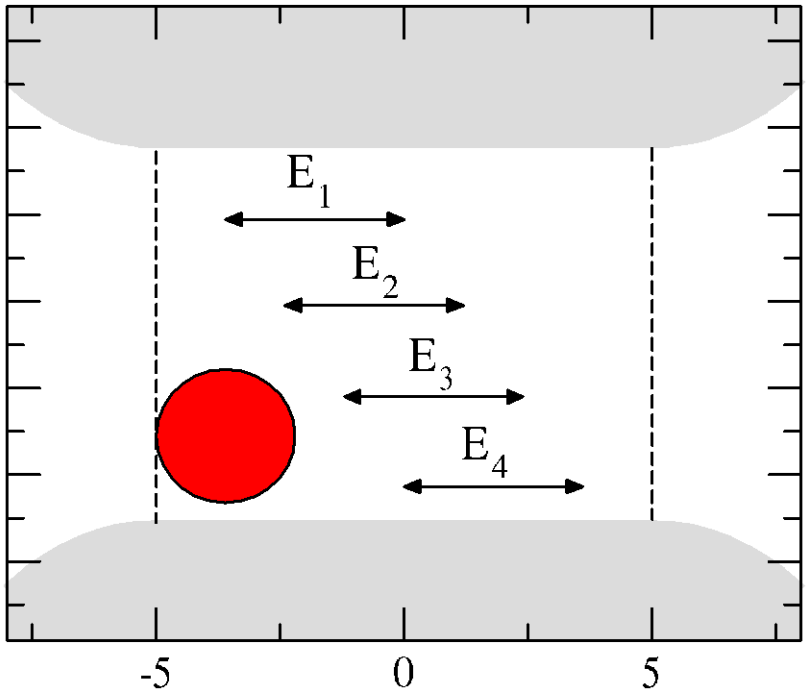

Fig. 2: In the 'restricted' case, four pairs of oxygen ions are restricted to four overlapping regions in the selectivity filter along the *z*-axis of the pore. The ion centers are restricted to the following intervals: E_1: [-3.6, 0], E_2: [-2.4, 1.2], E_3: [-1.2, 2.4], and E_4: [0, 3.6].

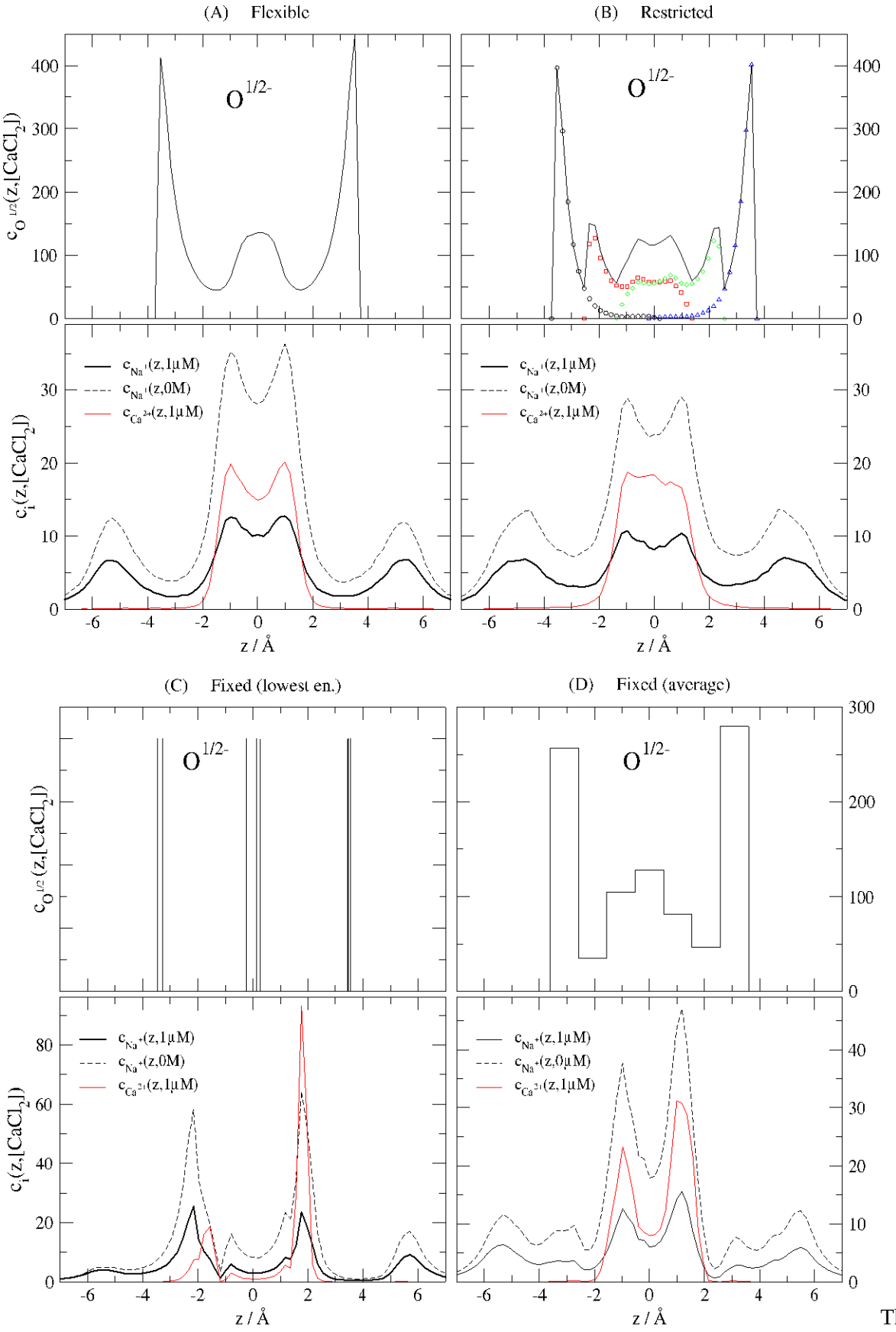
(A) Flexible
(B) Restricted
(C) Fixed (lowest en.)
(D) Fixed (average)
O 1/2-
c_O 1/2(z,[CaCl2])
c_i(z,[CaCl2])
c_Na+(z,1µM)
c_Na+(z,0M)
c_Ca2+(z,1µM)
z / Å

The

Fig. 3: Concentration profiles for oxygen (top row) and free ions (bottom row) for three different restrictions of the oxygens. (A) 'Flexible' case: the oxygen ions are fully mobile inside the selectivity filter, but cannot leave it. (B) 'Restricted' case: four pairs of oxygens are restricted to four overlapping regions inside the selectivity filter as shown in Fig. 2. Profiles with different symbols and colors in the top panel of Fig. 3B refer to these four oxygen pairs. The solid black line is the sum of these four profiles. (C) 'Fixed' case: the eight oxygens are fixed in positions that correspond to the lowest-energy configuration of a finite sample. The vertical lines in the top panel of Fig. 3C represent Dirac deltas corresponding to these fixed positions. In the bottom row, we show the profiles for Na^+ at $[CaCl_2] = 0$ M (dashed black line) and $[CaCl_2] = 10^{-6}$ M (thick solid black line). The thin solid red line represent the Ca^{2+} profiles for $[CaCl_2] = 10^{-6}$ M. (D) 'Average' case: is similar to Fig. 3C, but represents the averages of the ten low energy configurations.

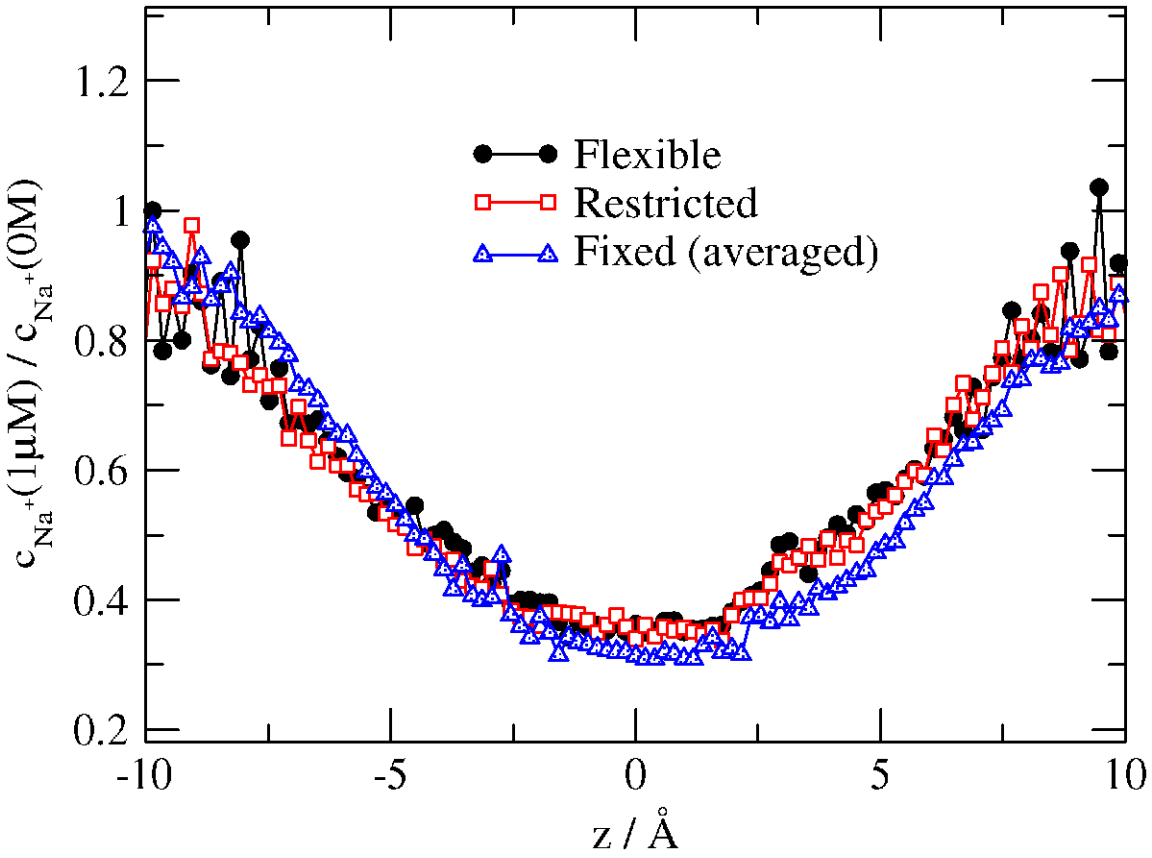

Fig. 4: The ratio of the Na^+ concentration profiles for $[CaCl_2] = 10^{-6}$ M and 0 M for the three cases depicted in Fig. 3.

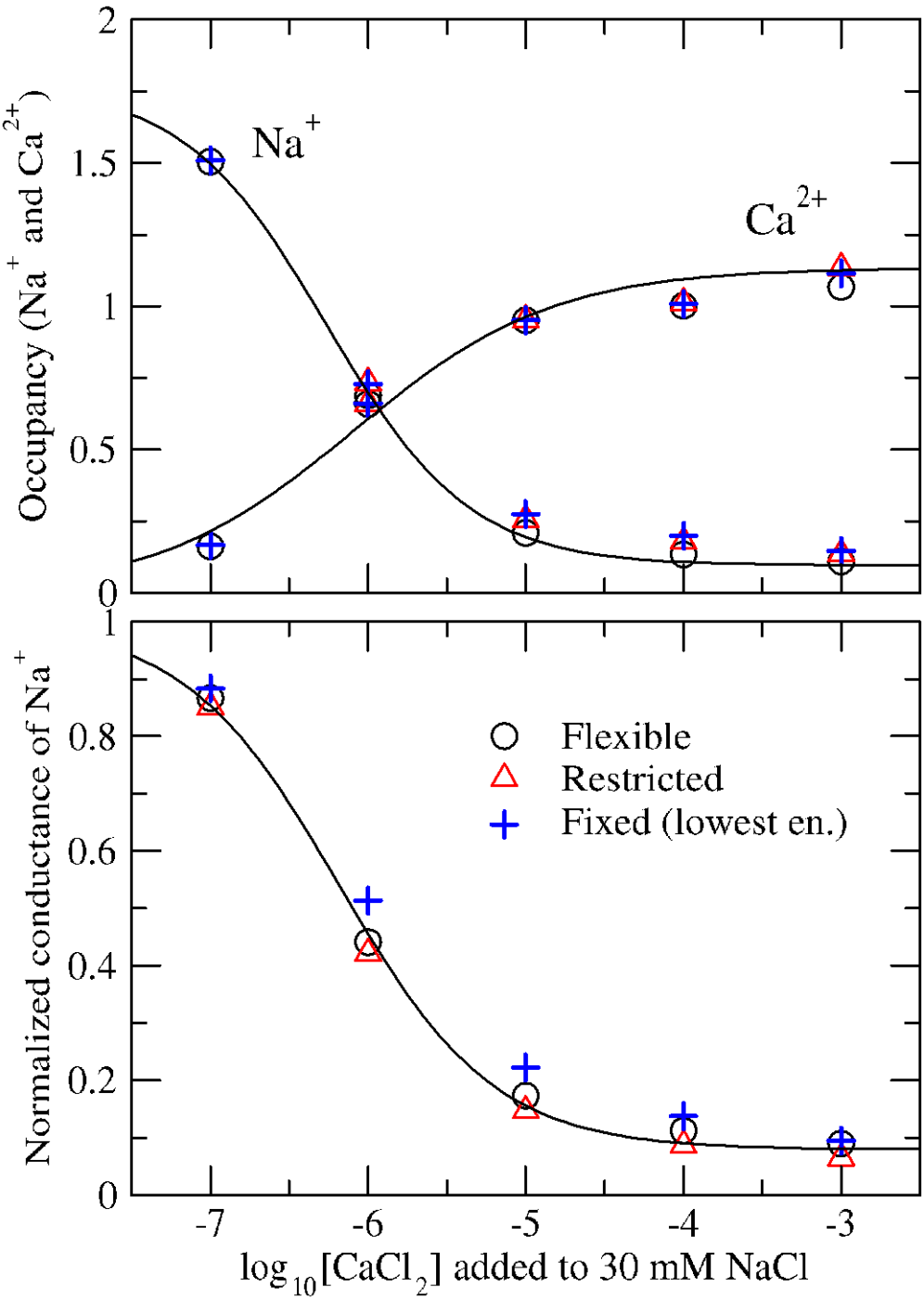

Fig. 5: (A) The average number (occupancy) of Na^+ (decreasing curves) and Ca^{2+} (increasing curves) ions as functions of $\log_{10}$ [$CaCl_2$] for the three different cases depicted in Fig. 3. (B) The conductance of Na+ ions normalized by the conductance at [$CaCl_2$] = 0 M as a function of $\log_{10}$ [$CaCl_2$] for the three different cases.

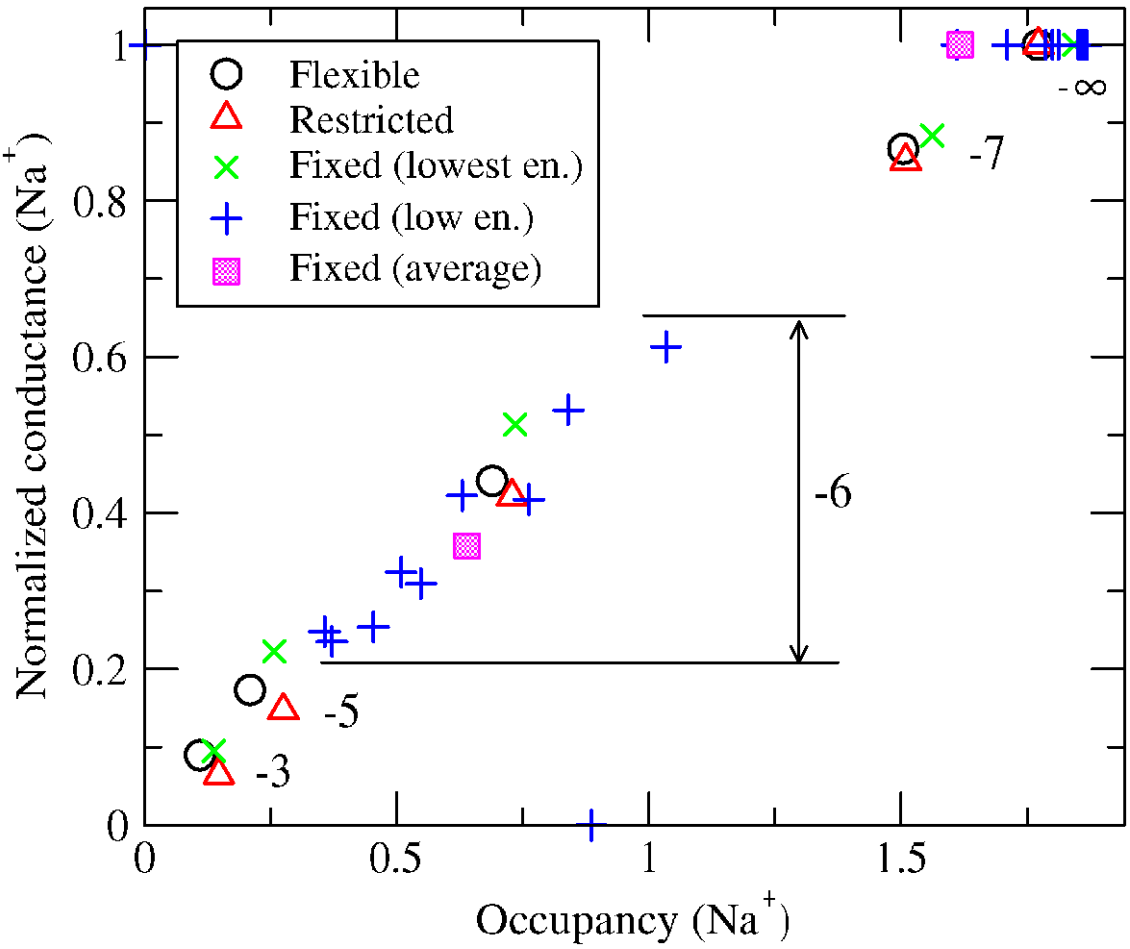

Fig. 6: Normalized conductance of Na^+ versus occupancy of Na^+ in the selectivity filter at different $CaCl_2$ concentrations for the three different cases depicted in Fig. 3. The green × symbols represent results for the lowest-energy 'fixed' oxygen configuration used in Fig. 3. The blue + symbols represent results for 10 selected 'fixed' oxygen configurations with low energies. The pink □ symbols represent averaged results for 10 selected 'fixed' oxygen configurations with low energies. The numbers near the symbol denote the values of $\log_{10}$ [$CaCl_2$]. Na^+-conductance for a given case is normalized by the Na^+-conductance for that particular case in the absence of Ca^{2+}.

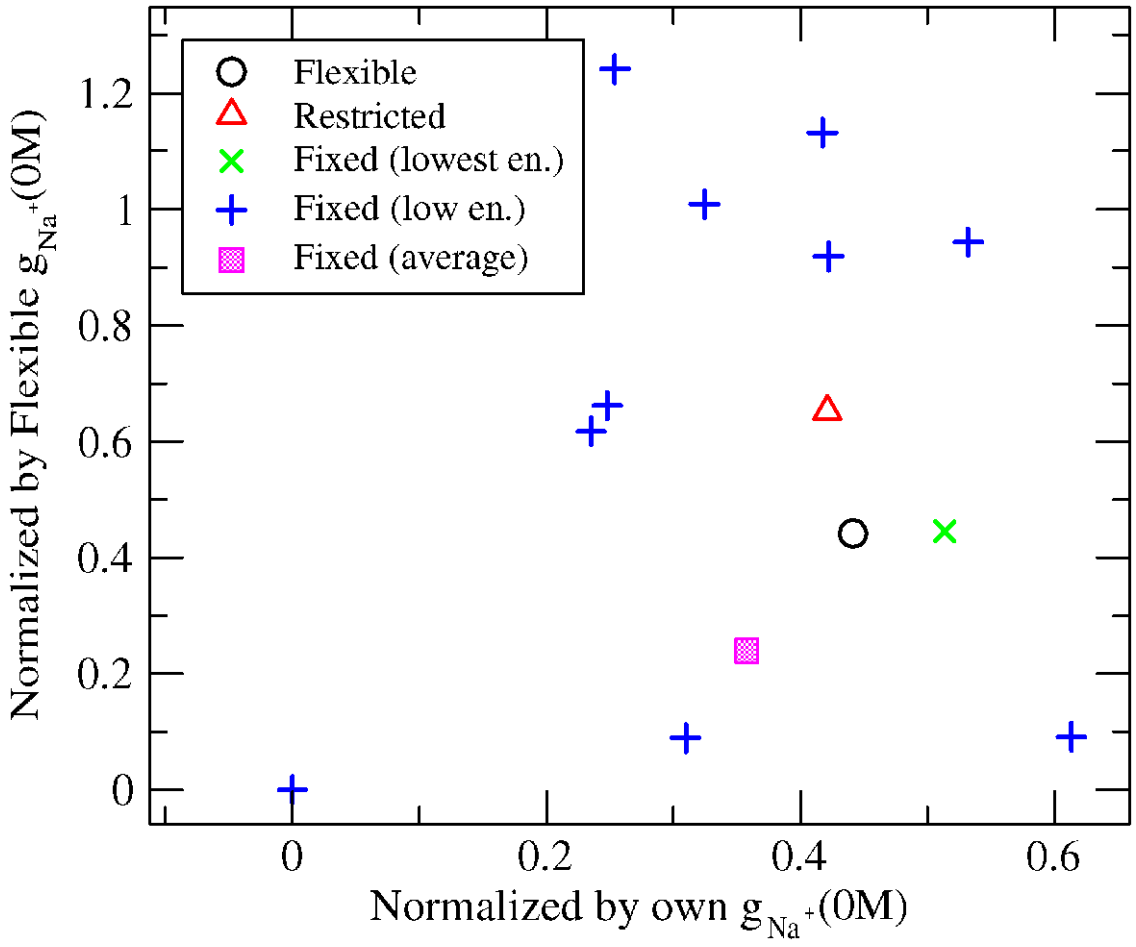

Fig. 7: Correlation between Na^+ conductances normalized by two different ways for $[CaCl_2] = 10^{-6}$ M. The ordinate shows conductance of Na^+ normalized by the Na^+ conductance in the absence of Ca^{2+} for the 'flexible' case. The abscissa shows conductance of Na^+ for a given case normalized by the Na^+ conductance in the absence of Ca^{2+} for that particular case. Symbols have the same meaning as in Fig. 6.

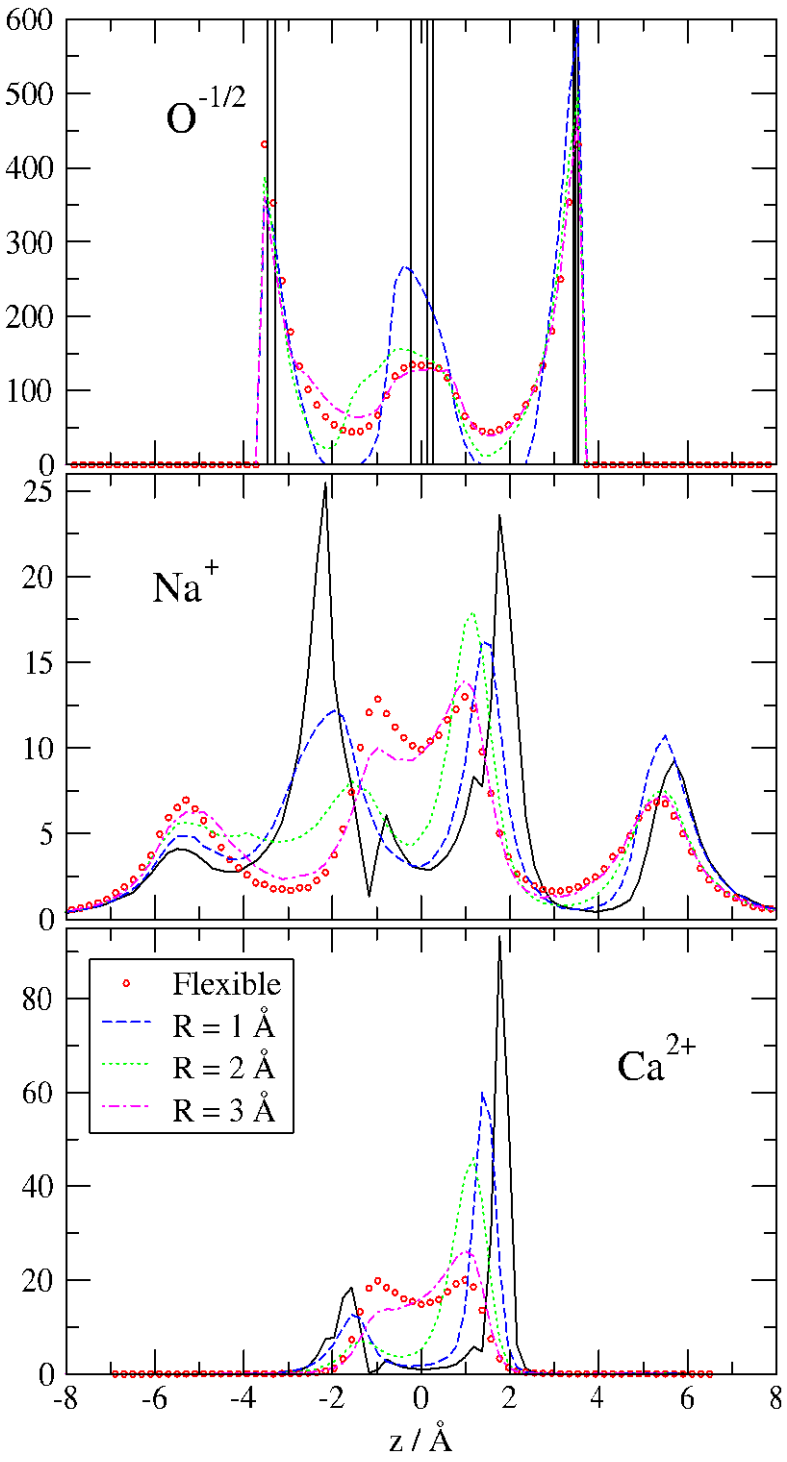

Fig. 8: Concentration profiles of $O^{-1/2}$, Na^{+}, and Ca^{2+} for the 'flexible' (red circles) and the lowest-energy 'fixed' (solid black line) cases, as well as cases when the oxygens are restricted in spheres of radii R_{ox} centered around the 'fixed' positions (various colored non-solid curves) at $[CaCl_2] = 10^{-6}$ M.

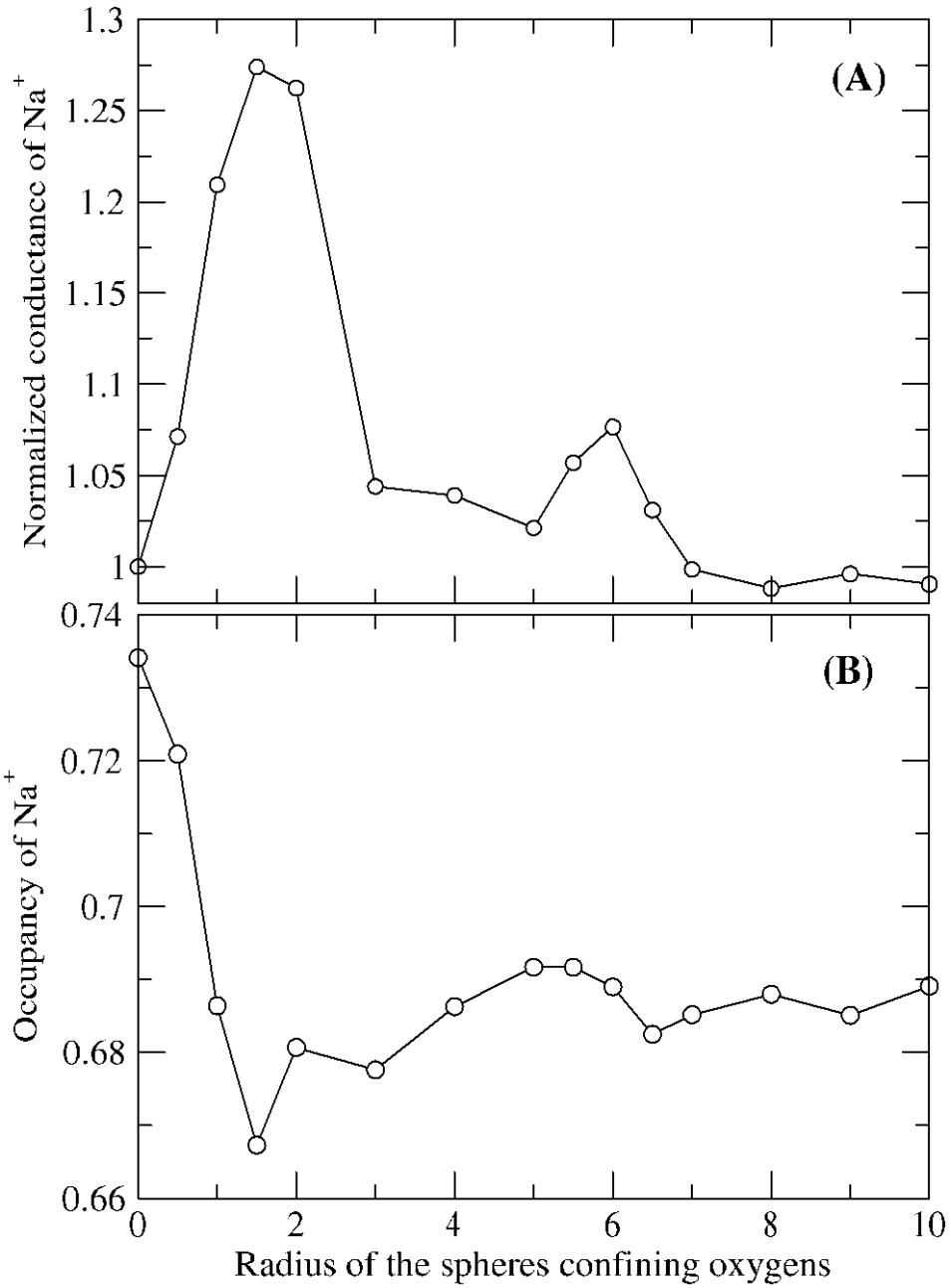

Fig. 9*:* (A) Normalized conductance and (B) occupancy of Na+ ions as functions of the spheres confining the oxygens R_{ox} for $[CaCl_2] = 10^{-6}$ M. The conductance is normalized by the 'fixed' (R_{ox} = 0 Å) case.